Reduction of lipid accumulation rescues Bietti's crystalline dystrophy phenotypes

Masayuki Hata[a,b], Hanako O. Ikeda[a,b,1], Sachiko Iwai[a], Yuto Iida[a], Norimoto Gotoh[a], Isao Asaka[c], Kazutaka Ikeda[d,e], Yosuke Isobe[d], Aya Hori[d], Saori Nakagawa[f], Susumu Yamato[f], Makoto Arita[d,e,g], Nagahisa Yoshimura[a,b], and Akitaka Tsujikawa[a]

[a]Department of Ophthalmology and Visual Sciences, Kyoto University Graduate School of Medicine, Kyoto 6068507, Japan; [b]Neuroprotective Treatment Project for Ocular Diseases, Institute for Advancement of Clinical and Translational Science, Kyoto University Hospital, Kyoto 6068507, Japan; [c]Department of Fundamental Cell Technology, Center for iPS Cell Research and Application, Kyoto University, Kyoto 6068507, Japan; [d]Laboratory for Metabolomics, RIKEN Center for Integrative Medical Sciences, Kanagawa 2300045, Japan; [e]Graduate School of Medical Life Science, Yokohama City University, Kanagawa 2300045, Japan; [f]Department of Bioanalytical Chemistry, Faculty of Pharmaceutical Sciences, Niigata University of Pharmacy and Applied Life Sciences, Niigata 9568603, Japan; and [g]Division of Physiological Chemistry and Metabolism, Graduate School of Pharmaceutical Sciences, Keio University, Tokyo 1058512, Japan

Edited by Paul S. Bernstein, University of Utah School of Medicine, Salt Lake City, UT, and accepted by Editorial Board Member Jeremy Nathans March 9, 2018 (received for review October 4, 2017)

Bietti's crystalline dystrophy (BCD) is an intractable and progressive chorioretinal degenerative disease caused by mutations in the *CYP4V2* gene, resulting in blindness in most patients. Although we and others have shown that retinal pigment epithelium (RPE) cells are primarily impaired in patients with BCD, the underlying mechanisms of RPE cell damage are still unclear because we lack access to appropriate disease models and to lesion-affected cells from patients with BCD. Here, we generated human RPE cells from induced pluripotent stem cells (iPSCs) derived from patients with BCD carrying a *CYP4V2* mutation and successfully established an in vitro model of BCD, i.e., BCD patient-specific iPSC-RPE cells. In this model, RPE cells showed degenerative changes of vacuolated cytoplasm similar to those in postmortem specimens from patients with BCD. BCD iPSC-RPE cells exhibited lysosomal dysfunction and impairment of autophagy flux, followed by cell death. Lipidomic analyses revealed the accumulation of glucosylceramide and free cholesterol in BCD-affected cells. Notably, we found that reducing free cholesterol by cyclodextrins or δ-tocopherol in RPE cells rescued BCD phenotypes, whereas glucosylceramide reduction did not affect the BCD phenotype. Our data provide evidence that reducing intracellular free cholesterol may have therapeutic efficacy in patients with BCD.

Bietti's crystalline dystrophy | cholesterol | *CYP4V2* gene | induced pluripotent stem cells | retinal pigment epithelium

Bietti's crystalline dystrophy (BCD) is an autosomal recessive, progressive chorioretinal degenerative disease (1). BCD is responsible for 10% of all cases of autosomal recessive retinal degeneration (2) and has higher prevalence in Asian, and especially in Japanese and Chinese, populations (3). Because no effective treatments are currently available, most patients with BCD develop decreased vision and visual field defects from the second decade of life that progress to legal blindness by the fifth or sixth decades of life. Therefore, development of treatments for BCD is urgently needed. Clinical characteristics of BCD include the emergence of yellow-white crystals in the cornea and fundus that are more numerous at the boundary between normal and atrophic-appearing retinal pigment epithelium (RPE) (4). In addition, RPE atrophy precedes photoreceptor atrophy in BCD (4, 5). These clinical findings suggest that RPE cells are primarily impaired in chorioretinal degeneration observed in patients with BCD (5, 6).

BCD was reported to be caused by mutations in the *CYP4V2* gene, of which the most common is the homozygous splice-site indel c.802-8_810del17insGC (3, 7). Whereas the normal *CYP4V2* gene encodes a 525-aa protein, this 17-bp deletion includes the exon 7 splice acceptor site and thus causes an in-frame deletion of exon 7 that results in the expression of a truncated 463-aa protein (3). The CYP4V2 protein, which is strongly expressed in RPE cells, is predicted to be a member of the cytochrome P450 superfamily and may be involved in the metabolism of lipids (3, 4, 8–11). However, the mechanisms of RPE damage in BCD remain largely unknown because of several problems associated with the research into BCD. In particular, lesioned cells cannot be readily acquired from BCD patients, and this circumstance makes it difficult to elucidate BCD pathophysiology and to develop effective therapeutic strategy.

Recent progress in cell-reprogramming technologies prompted us to consider a disease model based on induced pluripotent stem cells (iPSCs). We previously established stepwise differentiation of iPSCs into RPE (iPSC-RPE), and this differentiation system enabled us to isolate iPSC-RPE cells with high efficiency and extremely high purity (almost 100%) (12, 13). Thus, patient-specific iPSC-RPE cells enable more detailed investigations of the mechanisms underlying the onset and progression of BCD as well as drug screening.

In the present study, we generated human RPE cells from iPSCs derived from BCD patients carrying a *CYP4V2* mutation. We analyzed

Significance

Bietti's crystalline dystrophy (BCD) is an autosomal recessive, progressive chorioretinal degenerative disease. Retinal pigment epithelium (RPE) cells are impaired in patients with BCD, but the underlying mechanisms of RPE cell damage have not yet been determined because cells from lesions cannot be readily acquired from patients with BCD. In the present study, we successfully generated a human in vitro model of BCD, BCD patient-specific iPSC-RPE cells, and demonstrated that the accumulation of free cholesterol caused RPE cell damage and subsequent cell death via the induction of lysosomal dysfunction and impairment of autophagy flux in BCD-affected cells. We believe these findings provide evidence of the possible therapeutic efficacy of reducing intracellular free cholesterol in BCD.

Author contributions: M.H., H.O.I., N.G., M.A., N.Y., and A.T. designed research; M.H., H.O.I., S.I., Y. Iida, I.A., K.I., Y. Isobe, A.H., S.N., S.Y., M.A., N.Y., and A.T. performed research; I.A., A.H., S.N., and S.Y. contributed new reagents/analytic tools; M.H., H.O.I., S.I., Y. Iida, K.I., Y. Isobe, A.H., S.N., and S.Y. analyzed data; and M.H., H.O.I., S.I., Y. Iida, N.G., I.A., K.I., Y. Isobe, A.H., S.N., S.Y., M.A., N.Y., and A.T. wrote the paper.

Conflict of interest statement: Kyoto University has applied for patents related to this study (JP2017/90296) with M.H. and H.O.I. listed as inventors.

This article is a PNAS Direct Submission. P.S.B. is a guest editor invited by the Editorial Board.

[1]To whom correspondence should be addressed. Email: hanakoi@kuhp.kyoto-u.ac.jp.

This article contains supporting information online at www.pnas.org/lookup/suppl/doi:10.1073/pnas.1717338115/-/DCSupplemental.

Published online March 26, 2018.

phenotypes and lipid profiles of BCD patient-specific iPSC-RPE cells to investigate the mechanisms underlying the onset and progression of BCD. In addition, we sought to identify compounds that could rescue BCD-associated phenotypes.

Results

Generation of BCD Patient-Specific iPSCs and iPSC-Derived RPE Cells. We established iPSC lines from three BCD patients (BCD-1, BCD-2, and BCD-3) (Fig. S1) that carried the homozygous mutation indel c.802-8_810del17insGC (*CYP4V2* mut1) (Fig. S1) (7) in the *CYP4V2* gene and normal control (NOR) iPSC lines derived from three control individuals with normal fundus and without *CYP4V2* gene mutations. There were no remarkable differences between BCD and NOR iPSC lines during the establishment of iPSC preparations.

Thereafter, we induced BCD and NOR iPSCs to differentiate toward RPE cells (14). Differentiated iPSC-RPE cells with a polygonal, cobblestone-like morphology were cultured for over 90 d until high pigmentation appeared that indicated full functional maturity (Fig. 1*A*). The mRNA and protein levels of key RPE biomarkers, CRALBP and RPE65, were significantly elevated in differentiated RPE cells from both NOR and BCD iPSC cells compared with undifferentiated iPSC cells (Fig. S2). Notably, light microscopic examination revealed disturbances of BCD iPSC-RPE cell arrangement (Fig. 1*A*), as was confirmed with ZO-1 staining (Fig. 1*B*). Whereas the CYP4V2 protein was detected in NOR iPSC-RPE cells, it was not detected in BCD iPSC-RPE cells (Fig. 1*C*) despite similar CYP4V2 mRNA expression levels in NOR and BCD iPSC-RPE cells (Fig. S3). Furthermore, despite the redundancy in the activity of CYP4 family members (15), the mRNA expression levels of other genes from CYP4 family did not change in BCD iPSC-RPE cells compared with the levels seen in NOR iPSC-RPE cells (Fig. S3), indicating the absence of obvious compensatory changes in the expression of other CYP4 family members.

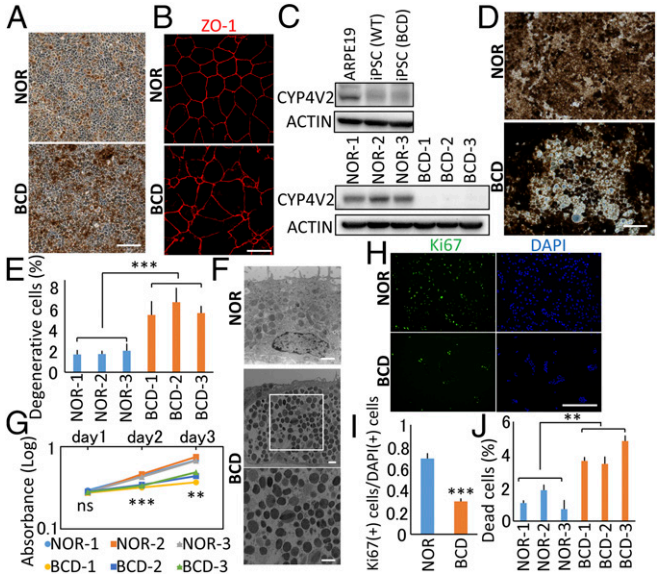

Fig. 1. Phenotypes of BCD patient-specific iPSC–RPE cells. (*A*) Bright-field micrographs taken after 3 mo of differentiation of BCD and NOR iPSCs into RPE cells (iPSC-RPE cells). (*B*) Immunocytochemical staining for ZO-1 in NOR and BCD iPSC-RPE cells. (*C*) Western blot analyses of CYP4V2 in a human RPE cell line (ARPE-19), NOR iPSCs, BCD iPSCs, NOR iPSC-RPE cells, and BCD iPSC-RPE cells. (*D*) Bright-field micrographs taken after 10 mo of differentiation of iPSCs into iPSC-RPE cells. (*E*) Evaluation of degenerative changes (having all the following features: vacuole formation, larger cell size, and pronounced pigmentation changes) in NOR and BCD iPSC-RPE cells. ***$P < 0.001$, BCD vs. NOR; Student's *t* test; $n = 3$ in each group. (*F*) TEM of NOR and BCD iPSC-RPE cells cultured for 10 mo. (*G*) Evaluation of the proliferation rate using the reaction with water-soluble tetrazolium salts. **$P = 0.003$, ***$P < 0.001$, BCD vs. NOR; Student's *t* test; $n = 3$ in each group. (*H* and *I*) Evaluation of the cell proliferation state using DAPI staining (blue) and immunocytochemical staining for Ki67 (green) in NOR and BCD iPSC-RPE progenitor cells. ***$P < 0.001$, BCD vs. NOR; Student's *t* test; $n = 4$ in each group. (*J*) Evaluation of cell death. **$P = 0.007$, BCD vs. NOR; Student's *t* test; $n = 3$ in each group. Error bars indicate SD. (Scale bars: 50 μm in *A*, *D*, and *H*; 10 μm in *B*; 1 μm in *F*.)

Morphological and Functional Analyses of BCD iPSC-RPE Cells. Remarkably, with time in culture, degenerative changes, such as vacuole formation, larger cell size, and pronounced pigmentation changes, were observed by phase-contrast microscopy in all lines of BCD iPSC-RPE cells (Fig. 1*D*). Compared with NOR iPSC-RPE cells, degenerative cells (which were defined as cells exhibiting all the following features: vacuole formation, larger cell size, and pronounced pigmentation changes) were seen significantly more frequently among BCD iPSC-RPE cells (Fig. 1*E*). Transmission electron microscopy (TEM) observations confirmed that NOR iPSC-RPE cells grew as a monolayer of highly polarized cells with abundant apical microvilli and melanosomes, whereas BCD iPSC-RPE cells exhibited accumulations of melanosomes and autophagosomes and intracellular pigmented granules and vacuolated cytoplasm (Fig. 1*F*) that recapitulated RPE changes reported in BCD patients (16). To better characterize the phenotype of iPSC-RPE cells, we evaluated the growth rate and cell death rate of iPSC-RPE progenitor cells (*Materials and Methods*). Compared with NOR iPSC-RPE progenitor cells, BCD iPSC-RPE progenitor cells showed a significantly lower rate of cell growth (Fig. 1*G*). To evaluate the state of cell proliferation, the numbers of $Ki67^+$ and $DAPI^+$ cells were counted, and the percentage of $Ki67^+/DAPI^+$ cells was evaluated. BCD iPSC-RPE progenitor cells showed a lower percentage of $Ki67^+$ cells in the $DAPI^+$ population (Fig. 1 *H* and *I*). Furthermore, we found a greater rate of cell death in BCD iPSC-RPE progenitor cells than in NOR iPSC-RPE progenitor cells (Fig. 1*J*).

To determine whether the cellular phenotypes observed in BCD iPSC-RPE cells were caused by the loss of function of the *CYP4V2* gene, we transferred wild-type *CYP4V2* (hereafter, *CYP4V2* WT), BCD mutant *CYP4V2* (hereafter, *CYP4V2* mut1), or a mock sequence (control) into BCD iPSC-RPE cells by a recombinant adenovirus vector (Fig. S4*A*). As expected, the CYP4V2 WT protein level increased only in BCD iPSC-RPE cells infected with *CYP4V2* WT, and the CYP4V2 mut1 protein level increased only in those infected with *CYP4V2* mut1 (Fig. S4*B*). CYP4V2 WT or mutant mRNA levels were elevated in BCD iPSC-RPE cells infected with *CYP4V2* WT and *CYP4V2* mut1 but not in those infected with the mock sequence (Fig. S4*C*). Compared with BCD iPSC-RPE cells infected with the mock sequence (control) or *CYP4V2* mut1, BCD iPSC-RPE cells infected with *CYP4V2* WT showed a significantly lower rate of degenerative changes, which were defined as described above (Fig. S4 *A* and *D*), and a higher rate of cell growth (Fig. S4*E*), indicating that the phenotypes observed in BCD iPSC-RPE cells were caused by the loss of function of the *CYP4V2* gene. To investigate whether other types of *CYP4V2* gene mutations may cause BCD phenotypes, we generated HEK293 cells with mutated *CYP4V2* using the CRISPR/Cas9 system. The introduced mutation (hereafter, *CYP4V2* mut2) caused a frame shift within exon 5 so that the mutated gene would encode only a very short protein (218 aa) (Fig. S4 *F* and *G*). Importantly, these *CYP4V2*-mutated HEK293 cells showed vacuole formation and subsequently had a higher death rate, i.e., degenerative changes similar to those observed in BCD iPSC-RPE cells (Fig. S4 *H*–*K*). Furthermore, transfection with *CYP4V2* WT adenovirus vector rescued the cellular phenotypes observed in *CYP4V2*-mutated HEK293 cells (Fig. S4 *L* and *M*).

Mechanisms of Cellular Damage in BCD iPSC-RPE Cells. Next, we investigated the mechanisms of degenerative changes found in BCD iPSC-RPE cells. From the findings of TEM examination, autophagy was suspected to be impaired in BCD. Therefore, we first evaluated the expression of the autophagy marker, microtubule-associated

MEDICAL SCIENCES

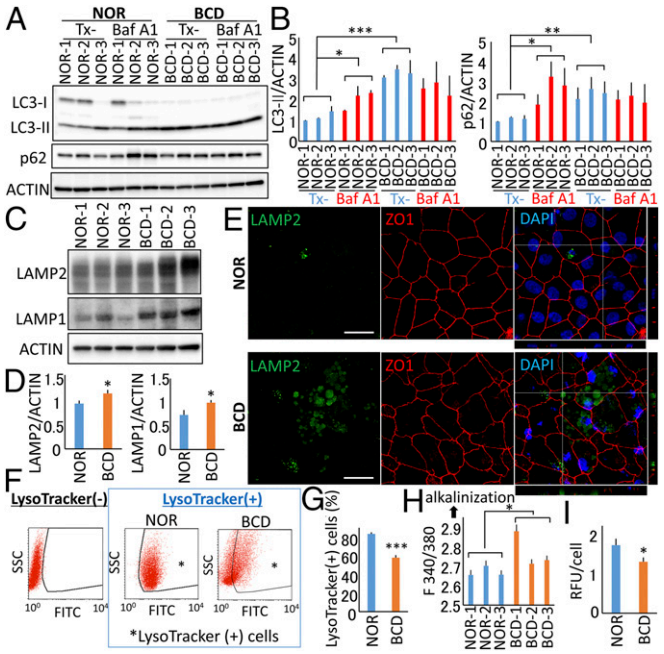

Fig. 2. Autophagy and lysosome function in NOR and BCD iPSC-RPE cells. (*A* and *B*) Expression of LC3-II and p62 with or without bafilomycin-A1 (Baf A1, 20 nM) in NOR and BCD iPSC-RPE cells. NOR Tx– vs. NOR with Baf A1: $*P = 0.0459$ (LC3-II) and $*P = 0.0496$ (p62), paired *t* test, $n = 3$ in each group; NOR Tx– vs. BCD Tx–: $***P < 0.001$ (LC3-II) and $**P = 0.0013$ (p62), Student's *t* test, $n = 3$ in each group. (*C* and *D*) Expression of LAMP1 and LAMP2. $*P < 0.05$; Student's *t* test; $n = 3$ derived from each of three lines. (*E*) Immunocytochemical staining for LAMP2 (green) and ZO1 (red). (Scale bars: 10 μm.) (*F* and *G*) FACS analysis of lysosome function using LysoTracker Green. $***P < 0.001$, BCD vs. NOR; Student's *t* test; $n = 3$ derived from each of three lines. (*H*) Lysosomal pH measurement using LysoSensor. The F340/380 ratio was determined. $*P = 0.0495$, BCD vs. NOR; Student's *t* test; $n = 3$ in each group. (*I*) The cathepsin D activity levels measured using a fluorometric cathepsin D activity assay. $*P = 0.032$, BCD vs. NOR; Student's *t* test; $n = 3$ derived from each of three lines. Error bars indicate SD.

protein 1 light chain 3 (LC3). C-terminal processing of LC3 produces LC3-I, which is modified to LC3-II with the initiation of autophagosome formation. We also measured p62/SQSTM1 (hereafter, p62) expression to assess autophagic flux (17, 18). Our data showed that the expression levels of LC3-II and p62 proteins were higher in BCD iPSC-RPE cells than in NOR iPSC-RPE cells, suggesting that autophagy was up-regulated and autophagic flux was impaired in BCD iPSC-RPE cells (Fig. 2 *A* and *B*). Further, bafilomycin-A1, an inhibitor of vacuolar H^+-ATPase, increased LC3-II and p62 protein levels in NOR iPSC-RPE cells (Fig. 2 *A* and *B*) but not in BCD iPSC-RPE cells. These observations indicated that autophagosomes accumulated because of the inhibition of autophagic degradation, e.g., via blockage of autophagosome–lysosome fusion and attenuation of lysosome content digestion (19, 20). Because p62 binds to LC3 and degrades upon fusion with the lysosome, we evaluated the expression of lysosome marker proteins. Analysis of mRNA expression levels of lysosome-associated genes showed that *LAMP2* was slightly up-regulated in BCD iPSC-RPE cells (Fig. S5). Compared with NOR iPSC-RPE cells, the levels of the lysosomal proteins LAMP1 and LAMP2 were significantly increased in BCD iPSC-RPE cells (Fig. 2 *C* and *D*). In addition, immunocytochemistry revealed that BCD iPSC-RPE cells showed excessive LAMP2 accumulation, indicating enlarged lysosomes (Fig. 2*E*).

Optimal lysosome function requires the ability to maintain acidic pH, and LysoTracker Green is a lysosomotropic dye that permits monitoring of pH-sensitive indices of the lysosomal function (21). We found that BCD iPSC-RPE cells showed a loss of LysoTracker signal compared with similar observations in NOR iPSC-RPE cells (Fig. 2 *F* and *G*). Lysosomal pH measurements using LysoSensor showed that the F340/380 ratio of fluorescence excited at 340 nm and 380 nm was higher (indicating a more alkaline state) in BCD iPSC-RPE cells than in NOR iPSC-RPE cells, indicating lysosomal alkalinization in BCD pathology (Fig. 2*H*). Further, the activity of cathepsin D, the primary aspartyl protease of the lysosome that has a particularly acidic pH optimum and pH-dependent maturation (22, 23), was impaired in BCD iPSC-RPE cells (Fig. 2*I*). Taken together, our findings indicate that the autophagic degradative system may be disturbed as a result of lysosomal dysfunction in BCD.

Lipidomic Analyses in BCD iPSC-RPE Cells. Because the CYP4V2 protein was predicted to be involved in lipid metabolism as a member of the cytochrome P450 superfamily, we performed comprehensive liquie choromatography (LC)-MS/MS–based lipidomic analyses. First, we evaluated the enzyme activity of CYP4V2 as a hydroxylase of polyunsaturated fatty acids (PUFAs) by using HEK293 cells overexpressing *CYP4V2* WT, *CYP4V2* mut1, and *CYP4V2* mut2. LC-MS/MS–based lipidomics showed that CYP4V2 WT protein possessed ω-hydroxylase and ω-1-hydroxylase activities (Fig. S6*A*), consistent with the previous report (9). However, the levels of those PUFA metabolites were under the detection limit in NOR and BCD iPSC-RPE cell culture media (Fig. S6*B*). Next, we performed untargeted lipidomics of NOR and BCD iPSC-RPE cells and found the accumulation of various glucosylceramides (GlcCer) and the reduction of cholesteryl esters in BCD iPSC-RPE cells (Fig. 3 *A* and *B*). We also determined the accumulation of free cholesterol per cell number in BCD iPSC-RPE cells (Fig. 3*C*). Filipin staining confirmed free cholesterol enrichment in BCD iPSC-RPE cells compared with NOR iPSC-RPE cells (Fig. 3*D*). These lipid profiles were similar to those observed in several types of lysosomal storage diseases, e.g., Niemann–Pick type C (NPC) or Gaucher's disease (24, 25). We also examined the mRNA expression levels of the causative genes of lysosomal storage diseases, genes involved in the metabolism/synthesis of glycolipids, and genes regulating intracellular cholesterol transport. *NPC1* was slightly up-regulated in BCD iPSC-RPE cells, but the expression levels of other genes did not differ between NOR and BCD iPSC-RPE cells (Fig. S5).

Dysfunctional reverse cholesterol transport due to abnormal *CYP27A1*, *CYP46A1*, and *CYP11A1* expression and *LXR* metabolism

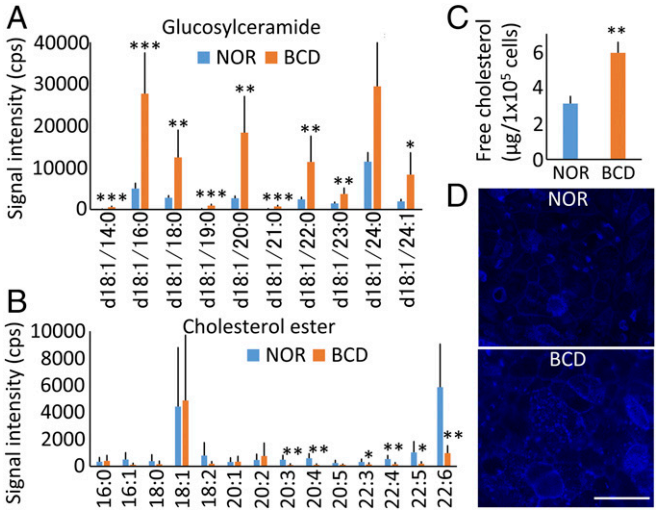

Fig. 3. Lipidomic analyses of NOR and BCD iPSC-RPE cells. (*A* and *B*) Untargeted lipidomics with LC-MS/MS in NOR and BCD iPSC-RPE cells. $*P < 0.05$, $**P < 0.01$, $***P < 0.001$, NOR vs. BCD; Student's *t* test; $n = 10$ and $n = 8$, respectively. (*C*) Free cholesterol concentration per cell number. $**P = 0.005$, NOR vs. BCD; Student's *t* test; $n = 3$ derived from each of three lines. Error bars indicate SD. (*D*) Filipin staining of iPSC-RPE cells. (Scale bar, 50 μm.)

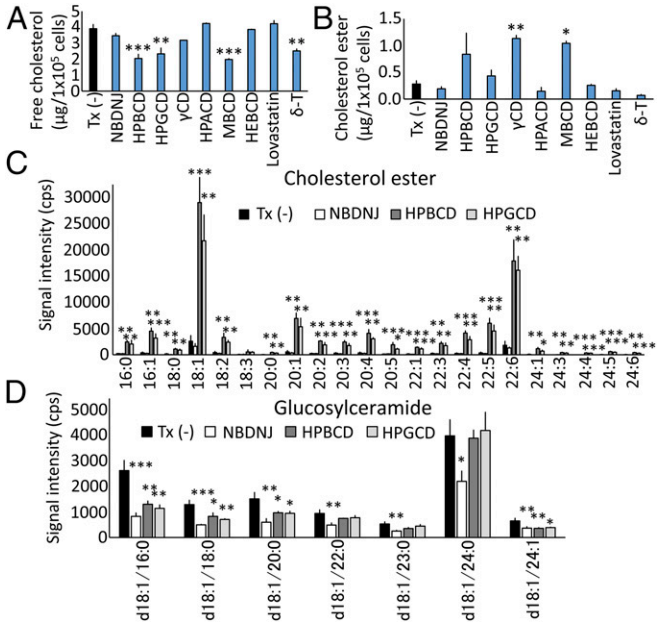

Fig. 4. Effect of CDs on lipids in BCD iPSC-RPE cells. (*A* and *B*) Therapeutic effects of NBDNJ, cyclodextrins (CDs), lovastatin, and δ-T on intracellular free cholesterol (*A*) or cholesteryl ester levels (*B*) in BCD iPSC-RPE cells derived from three lines. ***$P < 0.001$, **$P < 0.01$, *$P < 0.05$ vs. no treatment [Tx(–)]; one-way ANOVA followed by the Dunnett's test; $n = 3$. (*C* and *D*) LC-MS/MS–based lipidomic analyses of therapeutic effects of NBDNJ and CDs (HPBCD and HPGCD) on cholesteryl ester (*C*) or GlcCer (*D*). *$P < 0.05$, **$P < 0.01$, ***$P < 0.001$ vs. no treatment [Tx(–)]; one-way ANOVA followed by the Dunnett's test; $n = 3$.

is a well-known cause for retinal and RPE cell pathology (26–29). However, oxysterol levels did not differ significantly between NOR and BCD iPSC-RPE cells (Fig. S6*C*). Furthermore, mRNA levels of *CYP27A1*, *CYP46A1*, *CYP11A1*, and *LXR* did not differ between NOR and BCD iPSC-RPE cells (Fig. S5).

Therapeutic Effect of Lipid Accumulation Reduction on Phenotypes in BCD iPSC-RPE Cells. Because the accumulations of GlcCer and free cholesterol were observed in BCD iPSC-RPE cells, we investigated the effects of the reduction of lipid accumulation on BCD phenotypes. We tested several compounds, including cyclodextrins (CDs) (30–34), statin (35), and δ-tocopherol (δ-T) (36), which are known to reduce free cholesterol levels. We also tested the effect of N-butyldeoxynojirimycin (NBDNJ), which has been reported to reduce the GlcCer level (37). Our results showed that several CDs, namely 2-hydroxypropyl-β-CD (HPBCD), 2-hydroxypropyl-γ-CD (HPGCD), and methyl-β-CD (MBCD), as well as δ-T, reduced intracellular free cholesterol per cell number in BCD iPSC-RPE cells (Fig. 4*A*). Among them, HPBCD, HPGCD, and MBCD led to increases of cholesteryl ester levels per cell number, whereas δ-T caused a decrease of cholesteryl ester levels (Fig. 4 *B* and *C*). In contrast, NBDNJ, other CDs [γ-CD, 2-hydroxypropyl-α-CD (HPACD), and 2-hydroxyethyl-β-CD (HEBCD)], and lovastatin did not affect free cholesterol accumulation. Regarding the GlcCer level, as expected, lipidomic analysis showed that NBDNJ reduced GlcCer accumulation in BCD iPSC-RPE cells (Fig. 4*D*). Notably, the accumulation of GlcCer was also reduced by HPBCD and HPGCD.

Next, we investigated the therapeutic effects of these compounds on cellular phenotypes of BCD iPSC-RPE cells. HPBCD and HPGCD, which reduced free cholesterol per cell number, suppressed the development of degenerative changes in BCD iPSC-RPE cells (Fig. 5 *A* and *B*). This result was also supported by TEM examination, which showed a significant number of enlarged lysosomes with osmophilic structures in a clear matrix in nontreated BCD iPSC-RPE cells, but the amount of these hallmark structures in the cytosol was substantially lower in BCD iPSC-RPE cells treated with HPBCD (Fig. 5*C*). HPBCD and HPGCD also improved the cell growth rate and attenuated the cell death rate in BCD iPSC-RPE progenitor cells (Fig. 5 *D* and *E*). In contrast, NBDNJ, which reduced GlcCer but not free cholesterol levels per cell number, did not improve these cellular phenotypes. We also found that HPBCD and HPGCD tended to suppress the expression levels of LC3-II and p62 proteins in BCD iPSC-RPE cells, whereas NBDNJ was without effect (Fig. 5*F* and Fig. S7) In addition, HPBCD and HPGCD improved the LysoTracker signal in BCD iPSC-RPE cells, whereas NBDNJ did not (Fig. 5*G* and Fig. S7). In fact, HPBCD treatment decreased lysosomal pH in BCD iPSC-RPE cells as detected using LysoSensor; the improvement rates in the F340/380 ratio in BCD iPSC-RPE cells, defined as $[BCD_{\text{each line}}(\text{Tx}-) - BCD_{\text{each line}}(\text{HPBCD})]/[BCD_{\text{each line}}(\text{Tx}-) - NOR_{3\text{ lines average}}]$, where Tx– represents no treatment, were 67.7%, 80.0%, and 159.4% in the BCD-1, BCD-2, and BCD-3 cell lines, respectively. This indicated that the lysosomal alkalinization observed in the BCD iPSC-RPE cells was improved by HPBCD treatment. Thus, in agreement with the results of lipidomics, HPBCD and HPGCD reversed autophagic flux impairment and lysosomal dysfunction, but NBDNJ did not. These results imply that the cellular phenotypes observed in BCD iPSC-RPE cells were caused not by the accumulation of

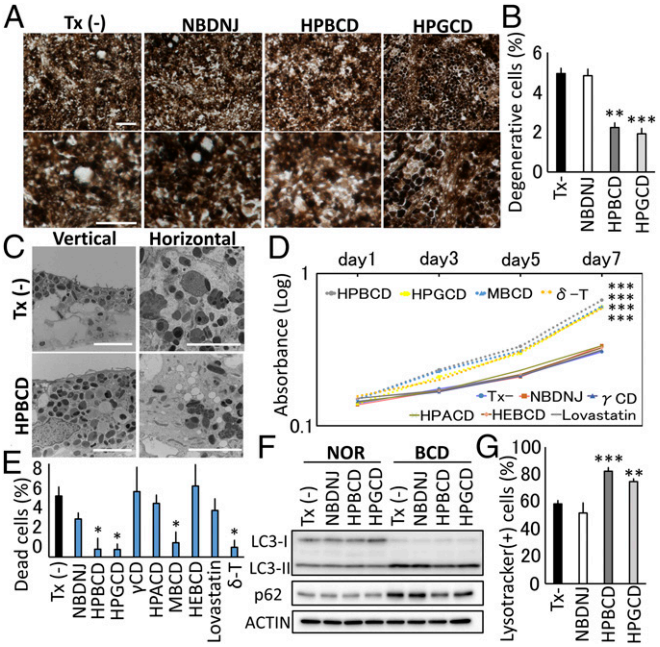

Fig. 5. Therapeutic effect of free cholesterol reduction on phenotypes in BCD iPSC-RPE cells. (*A*) Bright-field micrographs of BCD iPSC-RPE cells treated with CDs (HPBCD and HPGCD) or NBDNJ. (*B*) Evaluation of degenerative changes in BCD iPSC-RPE cells treated with CDs (HPBCD and HPGCD) or NBDNJ. **$P = 0.001$, ***$P < 0.001$ vs. no treatment [Tx(–)]; one-way ANOVA followed by the Dunnett's test; $n = 3$. (*C*) TEMs of BCD iPSC-RPE cells treated with HPBCD. (*D*) Evaluation of the proliferation rate in BCD iPSC-RPE progenitor cells treated with the indicated substances using the reaction with water-soluble tetrazolium salts. Day 7: ***$P < 0.001$ vs. no treatment [Tx(–)]; one-way ANOVA followed by Dunnett's test; $n = 4$ in each group. (*E*) Evaluation of cell death in BCD iPSC-RPE progenitor cells treated with the indicated substances. *$P < 0.05$ vs. no treatment [Tx(–)]; one-way ANOVA followed by the Dunnett's test; $n = 3$ in each group. (*F*) Therapeutic effects of the indicated substances on the abnormal autophagy parameters (LC3-II and p62) in BCD iPSC-RPE cells. (*G*) Therapeutic effects of the indicated substances on lysosome dysfunction in BCD iPSC-RPE cells using LysoTracker Green. ***$P = 0.0007$, **$P = 0.0019$ vs. no treatment [Tx(–)]; one-way ANOVA followed by Dunnett's test; $n = 3$ derived from each of three lines. Error bars indicate SD. (Scale bars: 50 μm in *A*; 5 μm in *C*.)

GlcCer but by the increase of free cholesterol level. On the contrary, HPBCD did not affect the percentages of degenerative cell and cell death or lysosome function in NOR iPSC-RPE cells (Fig. S8).

Discussion

In this study, we generated human iPSC-RPE cells derived from BCD patients carrying a *CYP4V2* mutation and successfully established a human in vitro model of BCD. In this model, RPE cells showed degenerative changes of vacuolated cytoplasm, i.e., a typical cellular phenotype observed in BCD. Using BCD iPSC-RPE cells, we revealed that in BCD the accumulation of free cholesterol was associated with lysosomal dysfunction due to lysosomal alkalinization and impairment of autophagy flux and thereby caused RPE cell damage followed by cell death. Based on this pathophysiology, we discovered that the reduction of free cholesterol in RPE cells rescued BCD phenotypes, which suggested that compounds that decrease the accumulation of free cholesterol could be therapeutic agents for BCD.

The difficulty in accessing human RPE and a lack of appropriate disease models have hampered efforts to investigate the pathology of BCD and to develop new drug candidates for this disease. The reported murine model for BCD (10) is not an entirely appropriate human BCD model for the following reasons. First, mice with the knockout of the *Cyp4v3* gene (the murine ortholog of *CYP4V3*, not *CYP4V2* itself) mainly exhibit impairment of photoreceptors but not of RPE, whereas clinical findings suggest that RPE is the primary lesion site in BCD (4, 6). Second, the chorioretinal impairment in these mutant mice is milder than that in human BCD. For understanding the underlying mechanism, HEK293 cells harboring the *CYP4V2* knockout were expected to be useful because of the degenerative changes observed in the mutant. However, a sufficient number of these mutant cells could not be collected for analysis of lipid profiles, as the *CYP4V2* knockout lowers the growth rate. In our experiments, BCD patient-specific iPSC-RPE cells recapitulated the cellular phenotypes of BCD patients. As a result, BCD iPSC-RPE cells provided a platform to investigate the pathophysiological mechanisms of lysosomal dysfunction and allowed identification of compounds that rescued the phenotypes associated with BCD.

In accordance with the high expression level of *CYP4V2* in RPE cells (9), BCD patients present with more severe RPE atrophy than photoreceptor atrophy, but it has been inconclusive whether *CYP4V2* mutation alone can cause RPE cells impairments. Our results revealed that the *CYP4V2* homozygous splice-site mutation indel c.802-8_810delinsGC, most commonly found in BCD, primarily caused RPE degenerative changes without interactions with the surrounding environment such as inflammatory cells or light-induced damage. This was also supported by the fact that *CYP4V2* transfection by recombinant adenovirus vector reversed degenerative changes in BCD iPSC-RPE cells, indicating that *CYP4V2* loss of function was a sufficient condition to induce the phenotypes observed in BCD iPSC-RPE cells.

In addition to RPE cells, *CYP4V2* is strongly expressed in various tissues, including the liver, kidney, and thyroid. Functional impairment of tissues other than the eye has not yet been reported in patients with BCD, possibly because careful histological characterization of additional tissues has not been performed. Our observation that the introduction of *CYP4V2* knockout in HEK cells caused cell degeneration indicates a systemic effect of the *CYP4V2* mutation. In fact, degenerative changes were observed in lymphocytes using TEM (4). Nevertheless, lymphocytes do not show strong functional consequences owing to their proliferative ability. In addition to their inability to divide, the phenotype appears easily in RPE, as an abundant lipid supply from both serum filtration and daily phagocytoses of photoreceptor outer segments highly activates lipid metabolism in RPE. This is also supported by our observation that the decrease in exogenous lipid load reduces the difference (Fig. S9*A*).

The present study provides evidence that the impairment of autophagic flux via lysosome dysfunction is a key event in BCD pathology. Autophagy, a process by which cellular constituents are degraded and recycled as part of normal cellular remodeling, is of particular importance in postmitotic cells with high metabolic demand, such as RPE cells (38, 39). BCD iPSC-RPE cells showed elevated levels of LC3-II and p62 proteins compared with those in NOR iPSC-RPE cells. The lysosomal inhibitor increased LC3-II and p62 levels in NOR iPSC-RPE cells but not in BCD iPSC-RPE cells. Our results also revealed accumulated and alkalinized lysosomes in BCD iPSC-RPE cells. Taken together, our results show that elevated lysosomal pH is the likely cause of autophagic flux impairment because the predominant lysosomal enzymes of the RPE cells are regulated by tight pH dependence. In fact, the activity of cathepsin D, the primary aspartyl protease of the lysosome, was impaired in BCD iPSC-RPE cells. Disruption of autophagy in postmitotic cells such as RPE would result in the accumulation of undigested or partially digested cellular aggregates, leading to degenerative cell death of RPE cells and secondary degeneration of the overlying photoreceptors (40, 41). The accumulation of pigmented granules observed in BCD iPSC-RPE cells also may be caused by lysosomal dysfunction (42).

Untargeted lipidomics revealed the accumulation of GlcCer and free cholesterol and the reduction of cholesteryl esters, which were similar to the lipid profiles of NPC (24). NPC is a lipid storage disease caused by mutations in the *NPC1* and *NPC2* genes, which encode proteins involved in cholesterol transport between lysosomes and endoplasmic reticulum (43, 44). In addition to the similar lipid profiles, BCD and NPC have common phenotypes, such as lysosome storage impairment, lysosome dysfunction, and autophagy flux impairment (34). Given that the reduction of free cholesterol improved the accumulation of GlcCer and lysosomal dysfunction in the present study, lysosome alkalinization may be a secondary phenomenon of cholesterol accumulation in the pathology of BCD. In contrast, reducing only the GlcCer level by NBDNJ did not improve lysosomal dysfunction, indicating that GlcCer accumulation may be a result rather than a cause of lysosomal dysfunction, as in the case of lysosomal storage diseases (45).

Among the compounds we tested, several CDs (HPBCD, HPGCD, and MBCD) and δ-T had positive therapeutic effects on the accumulation of free cholesterol. CDs, which are cyclic oligosaccharides composed of six to eight glucopyranosides, have a distinct barrel configuration with a hydrophilic exterior promoting water solubility and a hydrophobic interior that accommodates small lipophilic molecules. Some CDs have been reported to reduce the accumulation of free cholesterol and to increase life span in NPC models, possibly by working as a shuttle facilitating the egress of the trapped free cholesterol to intracellular sites for normal sterol processing (30–32, 34). In contrast, δ-T, a minor vitamin E species, appears to exert its effect in NPC models through the stimulation of lysosomal exocytosis (36). Importantly, although we observed that CDs and δ-T had opposite effects on cholesteryl ester levels, these compounds improved cellular phenotypes of BCD, indicating that therapies lowering intracellular free cholesterol could provide therapeutic benefit for BCD patients. With relevance to this point, HPBCD and HPGCD are currently in clinical trials as NPC treatments (33, 34). Thus, these are potential drug candidates for future treatment of BCD.

The lack of a proven mechanism linking CYP4V2 function and free cholesterol accumulation was a limitation of our study. CYP proteins have multiple functions, one of which is involvement in the metabolism of steroids. Given that several steroids have inhibitory effects on lysosomal cholesterol transport, resulting in phenotypes similar to those of NPC (46, 47), the disturbances in CYP4V2 protein functions may affect lysosomal cholesterol transport via steroid metabolism impairments. The other limitation was the potential influence of cell size on intracellular cholesterol content. The free cholesterol concentration per cell number was higher in BCD iPSC-RPE cells than in NOR iPSC-RPE cells. In contrast, normalization to protein content (owing to the larger RPE cell size in BCD pathology) could not clearly demonstrate whether free cholesterol content was significantly higher in BCD iPSC-RPE cells (Fig. S9*B*). Nevertheless, we

believe that higher content of free cholesterol per cell number is associated with BCD pathophysiology for the following reasons: (*i*) the cholesterol ester level apparently decreased in BCD iPSC-RPE cells; (*ii*) free cholesterol enrichment was demonstrated by filipin staining despite unknown localization; and (*iii*) treatments with HPBCD/HPGCD decreased free cholesterol content per cell in BCD iPSC-RPE cells, which corresponded to the improvements in BCD phenotype.

In summary, we successfully generated a human in vitro model of BCD, BCD iPSC-RPE cells, and unveiled the following mechanisms of cellular damage in BCD RPE cells: (*i*) the accumulation of free cholesterol that is associated with lysosomal impairments and (*ii*) lysosomal dysfunction that impaired autophagy flux and led to higher extent of RPE degenerative changes and cell death. Our data also provided evidence of the possible therapeutic efficacy of intracellular free cholesterol reduction for BCD patients.

Materials and Methods

This study followed the tenets of the Declaration of Helsinki and was approved by the Institutional Review Board of Kyoto University Graduate School of Medicine (G259 and R0091). After informed consent was obtained from three BCD patients with the homozygous mutation c.802-8_810del17insGC in the *CYP4V2* gene and from three control individuals with normal fundus and without *CYP4V2* gene mutations, fibroblast cell lines were generated. The method used for human iPSC generation was described previously (48). We analyzed three cell lines of BCD patients [BCD-1 (CiRA-j-0093-E), BCD-2 (CiRA-j-0094-G), and BCD-3 (CiRA-j-0095-B)] and three cell lines of NOR controls [NOR-1 (CiRA-j-0092-A), NOR-2 (CiRA-j-0156-A), and NOR-3 (CiRA-j-0157-A)].

Additional methods can be found in *SI Materials and Methods*.

ACKNOWLEDGMENTS. We thank Eri Kawaguchi and Kaori Misono (Kyoto University) for technical assistance; Akiko Hirata (Kyoto University) for the quantification of the number of cells with degenerative changes (vacuole formation and larger cells) and Ki67$^+$ cells; Dr. Jiro Usukura (Nagoya University) and Keiko Okamoto-Furuta and Haruyasu Kohda (Kyoto University) for helpful advice and technical support with electron microscopy; and Drs. Kenji Ishihara, Hiroomi Imamura, and Akira Kakizuka (Kyoto University) for helpful comments. This research was supported in part by research grants from Ono Medical Research Foundation, Novartis Pharma, Takeda Science Foundation, and the Japan National Society for the Prevention of Blindness; Grants-in-Aid for Young Scientists 15K20255 and17K16967 (to M.H.); Japan Society for the Promotion of Science Grants in Aid for Scientific Research JP16H01359 and JP16 K11285 (to H.O.I.) and JP15H05897, 15H05898, and 15H04648 (to M.A.); a grant from the Translational Research Network Program of the Japan Agency for Medical Research and Development (AMED) (to M.H.); and Grant 15652070 from the AMED Program for Intractable Diseases Research Utilizing Disease-Specific iPS cells (to I.A.).

1. Bietti GB (1937) Uber familiares Vorkommen von "retinitis punctata albescens" (verbunden mit "dystrophia marginalis cristallinza cornea"), Glitzern des Glaskorpers und anderen degenerativen Augenverunderungen. *Klin Monatsbl Augenheilkd* 99:737.
2. Mataftsi A, Zografos L, Millá E, Secrétan M, Munier FL (2004) Bietti's crystalline corneoretinal dystrophy: a cross-sectional study. *Retina* 24:416–426.
3. Li A, et al. (2004) Bietti crystalline corneoretinal dystrophy is caused by mutations in the novel gene CYP4V2. *Am J Hum Genet* 74:817–826.
4. Wilson DJ, Weleber RG, Klein ML, Welch RB, Green WR (1989) Bietti's crystalline dystrophy. A clinicopathologic correlative study. *Arch Ophthalmol* 107:213–221.
5. Halford S, et al. (2014) Detailed phenotypic and genotypic characterization of bietti crystalline dystrophy. *Ophthalmology* 121:1174–1184.
6. Miyata M, et al. (2016) Evaluation of photoreceptors in Bietti crystalline dystrophy with CYP4V2 mutations using adaptive optics scanning laser ophthalmoscopy. *Am J Ophthalmol* 161:196–205.e1.
7. Astuti GD, et al. (2015) Novel insights into the molecular pathogenesis of CYP4V2-associated Bietti's retinal dystrophy. *Mol Genet Genomic Med* 3:14–29.
8. Lee J, et al. (2001) The metabolism of fatty acids in human Bietti crystalline dystrophy. *Invest Ophthalmol Vis Sci* 42:1707–1714.
9. Nakano M, Kelly EJ, Wiek C, Hanenberg H, Rettie AE (2012) CYP4V2 in Bietti's crystalline dystrophy: ocular localization, metabolism of ω-3-polyunsaturated fatty acids, and functional deficit of the p.H331P variant. *Mol Pharmacol* 82:679–686.
10. Lockhart CM, Nakano M, Rettie AE, Kelly EJ (2014) Generation and characterization of a murine model of Bietti crystalline dystrophy. *Invest Ophthalmol Vis Sci* 55:5572–5581.
11. Nakano M, Kelly EJ, Rettie AE (2009) Expression and characterization of CYP4V2 as a fatty acid omega-hydroxylase. *Drug Metab Dispos* 37:2119–2122.
12. Osakada F, Ikeda H, Sasai Y, Takahashi M (2009) Stepwise differentiation of pluripotent stem cells into retinal cells. *Nat Protoc* 4:811–824.
13. Hirami Y, et al. (2009) Generation of retinal cells from mouse and human induced pluripotent stem cells. *Neurosci Lett* 458:126–131.
14. Sugita S, et al. (2015) Inhibition of T-cell activation by retinal pigment epithelial cells derived from induced pluripotent stem cells. *Invest Ophthalmol Vis Sci* 56:1051–1062.
15. Johnson AL, Edson KZ, Totah RA, Rettie AE (2015) Cytochrome P450 ω-hydroxylases in inflammation and cancer. *Adv Pharmacol* 74:223–262.
16. Furusato E, Cameron JD, Chan CC (2010) Evolution of cellular inclusions in Bietti's crystalline dystrophy. *Ophthalmol Eye Dis* 2010:9–15.
17. Kabeya Y, et al. (2000) LC3, a mammalian homologue of yeast Apg8p, is localized in autophagosome membranes after processing. *EMBO J* 19:5720–5728.
18. Komatsu M, et al. (2007) Homeostatic levels of p62 control cytoplasmic inclusion body formation in autophagy-deficient mice. *Cell* 131:1149–1163.
19. Mizushima N, Yoshimori T (2007) How to interpret LC3 immunoblotting. *Autophagy* 3:542–545.
20. Klionsky DJ, et al. (2016) Guidelines for the use and interpretation of assays for monitoring autophagy (3rd edition). *Autophagy* 12:1–222, and erratum (2016) 12:433.
21. Chazotte B (2011) Labeling lysosomes in live cells with LysoTracker. *Cold Spring Harb Protoc* 2011:pdb.prot5571.
22. Barrett AJ (1970) Cathepsin D. Purification of isoenzymes from human and chicken liver. *Biochem J* 117:601–607.
23. Rosenfeld MG, Kreibich G, Popov D, Kato K, Sabatini DD (1982) Biosynthesis of lysosomal hydrolases: their synthesis in bound polysomes and the role of co- and post-translational processing in determining their subcellular distribution. *J Cell Biol* 93:135–143.
24. Vanier MT, Millat G (2003) Niemann-Pick disease type C. *Clin Genet* 64:269–281.
25. Sillence DJ (2013) Glucosylceramide modulates endolysosomal pH in Gaucher disease. *Mol Genet Metab* 109:194–200.
26. Omarova S, et al. (2012) Abnormal vascularization in mouse retina with dysregulated retinal cholesterol homeostasis. *J Clin Invest* 122:3012–3023.
27. Pikuleva IA, Curcio CA (2014) Cholesterol in the retina: the best is yet to come. *Prog Retin Eye Res* 41:64–89.
28. Heo GY, Liao WL, Turko IV, Pikuleva IA (2012) Features of the retinal environment which affect the activities and product profile of cholesterol-metabolizing cytochromes P450 CYP27A1 and CYP11A1. *Arch Biochem Biophys* 518:119–126.
29. Saadane A, et al. (2014) Retinal and nonocular abnormalities in Cyp27a1(-/-)Cyp46a1(-/-) mice with dysfunctional metabolism of cholesterol. *Am J Pathol* 184:2403–2419.
30. Liu B, et al. (2009) Reversal of defective lysosomal transport in NPC disease ameliorates liver dysfunction and neurodegeneration in the npc1-/- mouse. *Proc Natl Acad Sci USA* 106:2377–2382.
31. Davidson CD, et al. (2009) Chronic cyclodextrin treatment of murine Niemann-Pick C disease ameliorates neuronal cholesterol and glycosphingolipid storage and disease progression. *PLoS One* 4:e6951.
32. Taylor AM, Liu B, Mari Y, Liu B, Repa JJ (2012) Cyclodextrin mediates rapid changes in lipid balance in Npc1-/- mice without carrying cholesterol through the bloodstream. *J Lipid Res* 53:2331–2342.
33. Tanaka Y, et al. (2015) Efficacy of 2-hydroxypropyl-β-cyclodextrin in Niemann-Pick disease type C model mice and its pharmacokinetic analysis in a patient with the disease. *Biol Pharm Bull* 38:844–851.
34. Soga M, et al. (2015) HPGCD outperforms HPBCD as a potential treatment for Niemann-Pick disease type C during disease modeling with iPS cells. *Stem Cells* 33:1075–1088.
35. Madra M, Sturley SL (2010) Niemann-Pick type C pathogenesis and treatment: from statins to sugars. *Clin Lipidol* 5:387–395.
36. Xu M, et al. (2012) δ-Tocopherol reduces lipid accumulation in Niemann-Pick type C1 and Wolman cholesterol storage disorders. *J Biol Chem* 287:39349–39360.
37. Cox T, et al. (2000) Novel oral treatment of Gaucher's disease with N-butyldeoxynojirimycin (OGT 918) to decrease substrate biosynthesis. *Lancet* 355:1481–1485.
38. Navone F, Genevini P, Borgese N (2015) Autophagy and neurodegeneration: Insights from a cultured cell model of ALS. *Cells* 4:354–386.
39. Frost LS, Mitchell CH, Boesze-Battaglia K (2014) Autophagy in the eye: implications for ocular cell health. *Exp Eye Res* 124:56–66.
40. Kaarniranta K, et al. (2013) Autophagy and heterophagy dysregulation leads to retinal pigment epithelium dysfunction and development of age-related macular degeneration. *Autophagy* 9:973–984.
41. Yao J, et al. (2015) Deletion of autophagy inducer RB1CC1 results in degeneration of the retinal pigment epithelium. *Autophagy* 11:939–953.
42. Schraermeyer U, Peters S, Thumann G, Kociok N, Heimann K (1999) Melanin granules of retinal pigment epithelium are connected with the lysosomal degradation pathway. *Exp Eye Res* 68:237–245.
43. Sleat DE, et al. (2004) Genetic evidence for nonredundant functional cooperativity between NPC1 and NPC2 in lipid transport. *Proc Natl Acad Sci USA* 101:5886–5891.
44. Kwon HJ, et al. (2009) Structure of N-terminal domain of NPC1 reveals distinct subdomains for binding and transfer of cholesterol. *Cell* 137:1213–1224.
45. Walkley SU, Vanier MT (2009) Secondary lipid accumulation in lysosomal disease. *Biochim Biophys Acta* 1793:726–736.
46. Aikawa K, Furuchi T, Fujimoto Y, Arai H, Inoue K (1994) Structure-specific inhibition of lysosomal cholesterol transport in macrophages by various steroids. *Biochim Biophys Acta* 1213:127–134.
47. Butler JD, et al. (1992) Progesterone blocks cholesterol translocation from lysosomes. *J Biol Chem* 267:23797–23805.
48. Takahashi K, et al. (2007) Induction of pluripotent stem cells from adult human fibroblasts by defined factors. *Cell* 131:861–872.